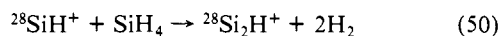


with high-temperature mass spectrometry. These lower values may be inaccurate due to the effect of hot bands on the measurement of  $\text{IP}(\text{Si}_2)$ .

$\text{Si}_2\text{H}^+$  ( $\text{Si}_2\text{D}^+$ ). The endothermicity of reaction 29, Table II, yields  $\Delta H_f^\circ(\text{Si}_2\text{H}^+) = 305.3 \pm 2$  kcal/mol. Reaction 31 gives a similar value for  $\Delta H_f^\circ(\text{Si}_2\text{D}^+)$  of  $303.6 \pm 2$  kcal/mol. We assume the difference in heats of formation of the protiated and deuteriated species is negligible. A third independent value of  $304.4 \pm 2$  kcal/mol is obtained from analysis of reaction 50, Table



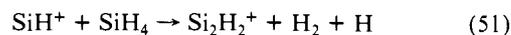
II. The average of these three values yields a best value for  $\Delta H_f^\circ(\text{Si}_2\text{H}^+)$  of  $304.4 \pm 1.6$  kcal/mol. Because of the competition with other  $\text{Si}_2\text{H}_n^+$  products, this is probably best viewed as an upper limit. The only literature values available for comparison come from electron-impact ionization measurements of  $\text{Si}_2\text{H}_6$ ,<sup>48,49</sup> However, the earlier work of Potzinger and Lampe<sup>48</sup> is flawed by the isotope overlap problem discussed above. The more recent measurements of Chatham et al.<sup>49</sup> are included in Table I.

$\text{Si}_2\text{H}_2^+$  ( $\text{Si}_2\text{D}_2^+$ ). The fact that formation of this product in reaction 32 (33) is exothermic gives an upper limit to  $\Delta H_f^\circ(\text{Si}_2\text{H}_2^+)$  of  $305.3 \pm 1.1$  kcal/mol ( $303.8 \pm 1.1$  for  $\text{Si}_2\text{D}_2^+$ ). A

(48) Potzinger, P.; Lampe, F. W. *J. Phys. Chem.* 1969, 73, 3912.

(49) Chatham, H.; Hils, D.; Robertson, R.; Gallagher, A. *J. Chem. Phys.* 1984, 81, 1770.

value of  $\leq 268.0 \pm 2.6$  kcal/mol is obtained from analysis of reaction 51, Table II. This value now gives the exothermicity



of reaction 32 as  $1.62 \pm 0.12$  eV. This heat of formation is lower than the value obtained by electron-impact ionization, Table I.<sup>49</sup> By use of our value and the heat of formation of  $\text{Si}_2\text{H}_2$  calculated by Ho et al.,<sup>9</sup>  $\text{IP}(\text{Si}_2\text{H}_2)$  is found to be  $\leq 7.68 \pm 0.16$  eV.

$\text{Si}_2\text{H}_3^+$  ( $\text{Si}_2\text{D}_3^+$ ). From the endothermicity of reaction 36 (38), Table II, comes  $\Delta H_f^\circ(\text{Si}_2\text{H}_3^+) = 266.3 \pm 2$  kcal/mol ( $264.9 \pm 1.5$  for  $\text{Si}_2\text{D}_3^+$ ). This does not agree very well with the value from electron-impact ionization,<sup>49</sup> Table I, although this has a very large error. The  $\text{IP}$  of  $\text{Si}_2\text{H}_3$  calculated by using this value and the calculated neutral heat of formation is given in Table IV.

**Acknowledgment.** This work was supported by the National Science Foundation (Grant No. CHE-8608847). B.H.B. is grateful to J. L. Elkind, N. Aristov, and K. M. Ervin for their help in conducting these experiments. We would like to thank Drs. R. Walsh, J. Berkowitz, and L. A. Curtiss for providing their papers before publication.

**Registry No.**  $\text{Si}^+$ , 14067-07-3;  $\text{SiH}_4$ , 7803-62-5;  $\text{Si}_2\text{H}_2^+$ , 39373-18-7;  $\text{SiH}$ , 13774-94-2;  $\text{SiH}_2$ , 13825-90-6;  $\text{SiH}_3$ , 13765-44-1;  $\text{SiH}_2^+$ , 28149-31-7;  $\text{SiH}_3^+$ , 41753-67-7;  $\text{Si}_2^+$ , 12597-36-3;  $\text{Si}_2\text{H}^+$ , 39373-15-4;  $\text{Si}_2\text{H}_3^+$ , 39373-99-4;  $\text{Si}_2$ , 12597-35-2;  $\text{Si}_2\text{H}$ , 102437-78-5;  $\text{Si}_2\text{H}_2$ , 36835-58-2;  $\text{Si}_2\text{H}_3$ , 12135-45-4.

## Spontaneously Organized Molecular Assemblies. 4. Structural Characterization of *n*-Alkyl Thiol Monolayers on Gold by Optical Ellipsometry, Infrared Spectroscopy, and Electrochemistry

Marc D. Porter,\*<sup>§†</sup> Thomas B. Bright,<sup>†</sup> David L. Allara,\*<sup>†</sup> and Christopher E. D. Chidsey<sup>†</sup>

Contribution from Bell Communications Research, Red Bank, New Jersey 07701, and AT&T Bell Laboratories, Murray Hill, New Jersey 07974. Received September 22, 1986

**Abstract:** Monolayer assemblies on *n*-alkyl thiols ( $\text{CH}_3(\text{CH}_2)_n\text{SH}$  where  $n = 1, 3, 5, 7, 9, 11, 15, 17,$  and  $21$ ), adsorbed on gold from dilute solution, have been characterized by optical ellipsometry, infrared (IR) spectroscopy, and electrochemistry. All three techniques show that there are distinct differences in structure between long- and short-chain thiol monolayers. The value of  $n$  for the sharpest change varies between 5 and 11 depending upon the specific measurement. The IR spectroscopic and ellipsometric data indicate that the long-chain thiols form a densely packed, crystalline-like assembly with fully extended alkyl chains tilted from the surface normal by  $20\text{--}30^\circ$ . As the chain length decreases, the structure becomes increasingly disordered with lower packing density and coverage. Electrochemical measurements of heterogeneous electron-transfer rates and of differential capacitance indicate that the long-chain monolayers are free of measurable pin holes, provide substantial barriers to electron transfer, and are strongly resistant to ion penetration. In contrast, with decreasing chain length the barrier properties become weaker. Taken together, these results demonstrate that monolayer assemblies of long-chain thiols on gold have significant potential as model systems for studies of heterogeneous electron transfer, ion transport, and double-layer phenomena.

The organization of monomolecular assemblies at solid surfaces provides a rational approach for fabricating interfaces with a well-defined composition, structure, and thickness. Such assemblies could provide a means to control the chemical and physical properties of interfaces for a variety of heterogeneous phenomena including catalysis,<sup>1-3</sup> corrosion,<sup>4</sup> lubrication,<sup>5,6</sup> and adhesion.<sup>7</sup> The ability to control interfacial processes has important implications from the point of view of both fundamental and technological

advances. For example, pin-hole-free, ionically insulating molecular films of monolayer thickness with well-defined structure

(1) Somorjai, G. A. *Chemistry in Two Dimensions: Surfaces*; Cornell University Press: Ithaca, NY, 1981.

(2) Murray, R. W. In *Electroanalytical Chemistry*; Bard, A. J., Ed.; Marcel Dekker: New York, 1984; Vol. 13.

(3) Durand, R. R.; Bencosme, C. S.; Collman, J. P.; Anson, F. C. *J. Am. Chem. Soc.* 1983, 105, 2710-2718.

(4) Notoya, T.; Poling, G. W. *Corrosion* 1979, 35, 193-200.

(5) Zisman, W. A. In *Friction and Wear*; Davies, R., Ed.; Elsevier: New York, 1959.

(6) Bowden, F. P.; Tabor, D. *The Friction and Lubrication of Solids*; Oxford University Press: London, 1968.

<sup>§</sup> Present address: Department of Chemistry, Iowa State University, Ames, Iowa 50011.

<sup>†</sup> Bell Communications Research.

<sup>‡</sup> AT&T Bell Laboratories.

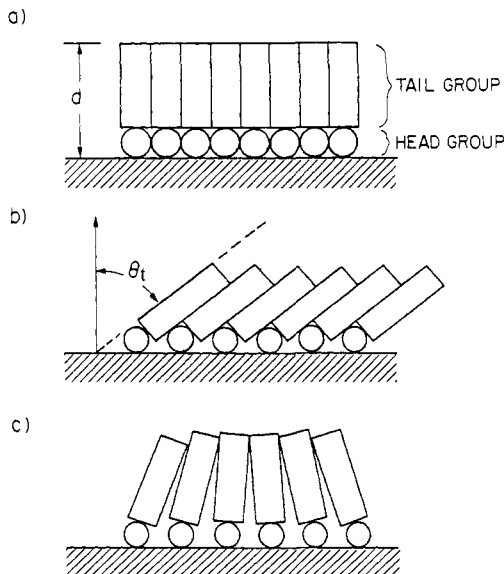


**Figure 1.** Structural models of an organized monolayer assembly: (a) closest packed arrangement of tail groups oriented normal to the substrate surface; (b) closest packed arrangement of head groups with the tail groups uniformly oriented at an angle  $\theta_t$  from the surface; and (c) closest packed arrangement of head groups with a distribution of tilted tail groups.

would provide an ideal surface for the study of simple electrode processes. A detailed understanding of charge-transfer mechanisms in such films would directly impact current efforts in biomembrane, electrochemistry, and microelectronics research.

As part of our interest in this area, we have been searching for approaches to study the fundamental chemical and physical interactions that control the formation, structure, and reactivity of chemically modified surfaces. This has consisted, in part, of selecting molecular systems that provide the means to probe those interactions that govern the attachment, orientation, and packing density of the surface species and, in part, of searching for informative characterization tools to apply to these systems. Further, it has become increasingly clear that characterization of defect structures, as well as average molecular structures, is an important issue which needs to be addressed in many applications. The types of interactions which are most relevant to these structural aspects include the bonding interactions and registry between the head group and the substrate and the intermolecular interactions between adjacent adsorbate molecules.<sup>8-10</sup> Figure 1 summarizes three idealized structures for organized monolayer assemblies of typical amphiphilic molecules, based on the aforementioned considerations and also on various studies, particularly those using electron diffraction.<sup>11-13</sup> In general, the greater the mismatch between the van der Waals radii of the tail groups and the head groups and between these quantities and the substrate lattice parameters, the greater the tendency for the monolayer to deviate from well-arranged structures such as in Figures 1a and 1b and to exhibit structural disorder and defects. The structure in Figure 1c could arise, for example, with an assembly in which the substrate imposes a head-group spacing leading to lower density than a closest packed arrangement. In this case, a final structure could arise as a compromise between a tendency for tails to pack parallel to one another and be oriented perpendicular to the surface (e.g., in order to maximize interlocking interactions of CH<sub>2</sub> groups in

an alkyl chain) and a tendency for the head groups to maintain an open structure for which parallel, tilted tails (Figure 1b) do not pack optimally (e.g., poorly interlocking interactions of CH<sub>2</sub> units). Detailing the above underlying structural factors responsible for stabilizing such structures poses a complex problem, particularly for the analysis of structural defects such as those expected in the structure in Figure 1c. In addition, with the current understanding of the physics and chemistry of such assemblies, it is unlikely that a single adsorbate-substrate system can be identified to probe all of these interactions. It follows that the most effective approach to the study of the fundamental aspects of the formation and structure of monomolecular assemblies is to select a variety of adsorbate systems which can serve as models for examining some simple combination of the aforementioned interactions.

Several systems possess the requisite properties of an experimental model. Previous studies have shown the utility of siloxy,<sup>2,14,15</sup> acid/base,<sup>16-19</sup> and charge-transfer<sup>20-22</sup> chemistry for attaching a variety of molecules at both metallic and nonmetallic surfaces. A particularly detailed series of studies has examined the effects of the size and functionality of substituent groups on the orientation, surface concentration, and electrochemical reactivity of aromatic molecules adsorbed at platinum.<sup>20-22</sup> Other investigations have shown the importance of the alkyl chain length of alkanic acids on the orientation and bonding at ambient surfaces of aluminum and silver<sup>19,23</sup> and at metallic copper.<sup>24</sup> Another attractive system is based on the adsorption of *n*-alkyl organosulfur compounds on noble metals such as gold.<sup>25-27</sup> This system has several advantages as a model, including the choice of thiol, sulfide, or disulfide functionalities to study head-group/substrate interactions and the variation of the chain length to study the importance of tail interactions. In addition, a metallic substrate with a low chemical reactivity, such as gold, provides the opportunity to apply both vibrational spectroscopic and electrochemical techniques. The combination of these techniques is effective at probing the averaged bulk structure and the extent of defects in monolayer films.

In this study we present results on the structural characterization of self-assembled monomolecular assemblies of *n*-alkyl thiols on polycrystalline gold. The importance of the alkyl chain length on the packing density, intermolecular environment, and geometry of the monomolecular assemblies are of particular interest. Infrared spectroscopy and ellipsometry are used to probe the "average" molecular structure of the assemblies, including thickness, packing density, crystalline environment, and orientation. Electrochemical capacitance and heterogeneous electron-transfer measurements are used to examine the microscopic integrity (relative to structural defects) of the assemblies. The correlation between the data from the photon and electrochemical probes indicates a distinct influence of the length of the alkyl chain on the structure and surface concentration of the monomolecular assembly. The electrochemical measurements also demonstrate

(7) Kaelble, D. H. *Physical Chemistry of Adhesion*; Wiley-Interscience: New York, 1971.

(8) Langmuir, I. *J. Chem. Phys.* **1933**, *1*, 756-776.

(9) Epstein, H. T. *J. Phys. Colloid Chem.* **1950**, *1053*-1069.

(10) Safran, S. A.; Robbins, M. O.; Garoff, S. *Phys. Rev. A* **1986**, *33*, 2186-2189.

(11) See ref 6, Part I, Chapter 10; Part II, Chapter 18.

(12) Chapman, J. A.; Tabor, D. *Proc. R. Soc. London* **1957**, *242*, 96-107.

(13) Garoff, S.; Deckman, H. W.; Dunsmuir, J. H.; Alvarez, M. S. *J. Phys. (Paris)* **1986**, *47*, 701-709.

(14) Moses, P. R.; Wier, L.; Murray, R. W. *Anal. Chem.* **1975**, *47*, 1882-1886.

(15) Gun, J.; Iscovici, R.; Sagiv, J. *J. Colloid Sci.* **1984**, *101*, 201-213.

(16) Bigelow, W. C.; Pickett, D. L.; Zisman, W. A. *J. Colloid Sci.* **1946**, *1*, 513-538.

(17) Polymeropoulos, E. E.; Sagiv, J. *J. Chem. Phys.* **1978**, *69*, 1836.

(18) Golden, W. G.; Snyder, C.; Smith, B. *J. Phys. Chem.* **1982**, *86*, 4675-4678.

(19) (a) Allara, D. L.; Nuzzo, R. G. *Langmuir* **1985**, *1*, 45-52. (b) Allara, D. L.; Nuzzo, R. G. *Ibid.* **1985**, *1*, 52-66.

(20) Soriaga, M. P.; Hubbard, A. T. *J. Am. Chem. Soc.* **1982**, *104*, 3937-3945.

(21) Soriaga, M. P.; Hubbard, A. T. *J. Am. Chem. Soc.* **1982**, *104*, 2735-2742.

(22) Chia, V.; Soriaga, M. P.; Hubbard, A. T. *J. Electroanal. Chem.* **1984**, *169*, 97-106.

(23) Porter, M. D.; Allara, D. L.; Bright, T. B.; Nuzzo, R. G., manuscript in preparation.

(24) DuBois, L. H.; Zegarski, B. R.; Nuzzo, R. G. *Langmuir* **1986**, *2*, 412-417.

(25) Nuzzo, R. G.; Allara, D. L. *J. Am. Chem. Soc.* **1983**, *105*, 4481-4483.

(26) Li, T. T. T.; Weaver, M. J. *J. Am. Chem. Soc.* **1984**, *106*, 6107-6108.

(27) Whitesides, G.; Troughton, B., personal communication.

the potential utility of these assemblies as model systems for studying heterogeneous electron transfer, ion transport, and double-layer phenomena. A brief discussion of these possibilities is given.

### Experimental Section

**Self-Assembly of Alkyl Thiols at Gold.** The alkyl thiol assemblies were spontaneously absorbed<sup>25</sup> by immersing freshly evaporated gold into dilute (0.1–1.0 mM) alkyl thiol solutions of hexadecane or absolute ethanol. For the 2-in. diameter surface of our standard substrate and for a monolayer coverage of  $\sim 10^{14}$  molecules/cm<sup>2</sup>, those concentrations represent an approximately  $10^3$ - to  $10^4$ -fold excess of reagent for complete monolayer conversion. The hexadecane was purified by column chromatography just prior to use with activity-one alumina. The ethanol was commercial reagent grade (unadulterated) and used without further purification. Absolute methanol as well as other pure solvents such as CHCl<sub>3</sub> give similar results. The procedures used are quite similar to those for a previous preparation of carboxylic acids on aluminum.<sup>19a</sup> The alkyl thiols ( $n = 1, 3, 5, 7, 9, 11, 15,$  and  $17$ ) were used as received (Aldrich Chemical Co. Milwaukee, WI). The CH<sub>3</sub>(CH<sub>2</sub>)<sub>21</sub>SH was a gift from B. Troughton and G. Whitesides (Department of Chemistry, Harvard University). The thiols with  $n = 5, 7, 9,$  and  $11$  showed approximately 2% disulfide impurity by GC/MS analysis and <0.5% of other observable impurities. For the  $n = 15$  and  $17$  thiols, the disulfides were not sufficiently volatile for analysis but the observable impurities were again <0.5%. The progress of the formation of the self-assembled structures was monitored by ellipsometry. Rinses with absolute ethanol and hexane (HPLC grade) were used to remove residual solvent and adsorbate.

The substrates were prepared by the resistive evaporation of chromium and gold (99.99% purity) onto 2-in. silicon wafers at about  $1 \times 10^{-7}$  torr in a cryogenically pumped deposition chamber. Thicknesses, monitored with a quartz oscillator, were typically 15–20 and 150–200 nm for chromium and gold, respectively. The deposition of chromium prior to that of gold was performed to enhance adhesion to the substrate. The silicon was precleaned in hot 1:4 H<sub>2</sub>O<sub>2</sub> (30%)/H<sub>2</sub>SO<sub>4</sub> and rinsed with distilled-deionized H<sub>2</sub>O and absolute ethanol. After deposition, the chamber was back-filled with prepurified nitrogen.

**Ellipsometric Film-Thickness Measurements.** The thicknesses of the films were determined with ellipsometry. A Rudolph Model 423 null-point ellipsometer (Rudolph Instruments, Fairfield, NJ) was used to measure the analyzer and polarizer angles of the substrate at 632.8 nm immediately after removal from the deposition chamber. The complex refractive indexes for the substrates were calculated with the two-phase parallel-layer model from classical electromagnetic theory.<sup>28–30</sup> After film formation, the samples were again analyzed and the thicknesses of the film determined from a three-phase model using a real refractive index of 1.45 (the imaginary part of the complex refractive index equals zero as the alkyl thiols are transparent at 6328 Å) for the monolayer and the previously measured complex refractive indexes for the substrate. Algorithms for these calculations have been previously described.<sup>19b</sup>

**Infrared External Reflection Spectroscopy Analysis.** Absorption spectra were obtained in a single reflection mode using a nitrogen-purged Digilab 15-E Fourier transform infrared spectrometer (Bio-Rad, Cambridge, MA). The p-polarized light was incident at 86°. A narrow-band MCT detector, cooled with liquid nitrogen, was used to detect the reflected light. After triangular apodization, the spectral resolution was 2 cm<sup>-1</sup>. The moving mirror speed was 1.4 cm/s. All spectra are reported as the  $-\log(R/R_0)$  where  $R$  is the reflectivity of the monolayer at gold and  $R_0$  is the reflectivity of a bare gold reference substrate. These gold reference substrates were cleaned using a previously described procedure<sup>19b</sup> which consisted of sequential washes in hot 1:4 H<sub>2</sub>O<sub>2</sub> (30%)/H<sub>2</sub>SO<sub>4</sub>, 30% H<sub>2</sub>O<sub>2</sub>, and distilled deionized H<sub>2</sub>O.

**Electrochemical Measurements.** Cyclic voltammetry was performed with a Pine RDE3 or PAR 173/175 potentiostat/universal programmer. Data were obtained with a Hewlett-Packard 7090A or a Houston 2000 X-Y recorder. The gold substrates were mounted in a conventional three-electrode cell with an exposed area of 0.32 cm<sup>2</sup>. Solutions were purged with prepurified nitrogen or argon. All potentials were measured and reported with respect to a Ag/AgCl (saturated KCl) reference electrode. Solutions were prepared immediately before use with deionized H<sub>2</sub>O from a Milli-Q purification system (Millipore Products, Bedford,

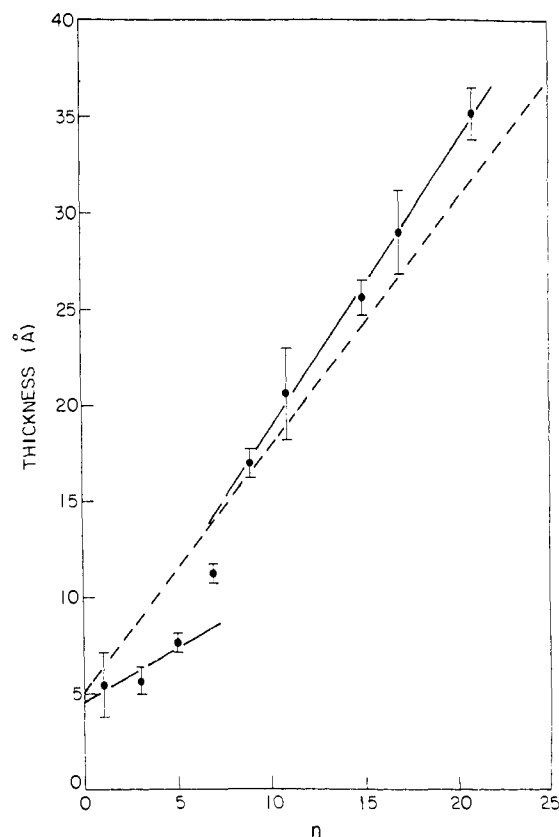


**Figure 2.** Film thicknesses for  $n$ -alkyl thiols adsorbed at gold; the ellipsometrically determined thickness (—) and estimated thickness for a fully extended chain normal to the surface, in Å (---), are plotted against the number of methylene groups in the chain,  $n$ .

MA). The KCl, HClO<sub>4</sub>, NaF, K<sub>3</sub>Fe(CN)<sub>6</sub>, and Fe(NH<sub>4</sub>)(SO<sub>4</sub>)<sub>2</sub> were reagent grade.

### Results and Discussion

**Characterization with Optical Ellipsometry.** Optical ellipsometry was applied as a convenient and precise means of determining the average monolayer thicknesses of the films and following the progress of film growth. These data are shown in Figure 2. The abscissa,  $n$ , is the number of CH<sub>2</sub> groups in the alkyl chain. The thicknesses are reported as the average of 8–10 trials with the uncertainty given as the standard deviation. The measured thicknesses show two apparent regions of dependence on  $n$ . The region between  $n = 1$  and  $n = 9$  shows substantial curvature. Linear regression analysis of the data between  $n = 1$  and  $n = 5$  yields values for the slope and intercept of 0.56 Å per CH<sub>2</sub> group and 4.6 Å, respectively. The region between  $n = 9$  and  $n = 21$  is linear and gives a slope of 1.5 Å per CH<sub>2</sub> group and an intercept equal to 3.8 Å. In order to relate these data to a simple structural model, thicknesses were calculated for an ideal film consisting of  $n$ -alkyl thiols fully extended in an all-trans conformation perpendicular to the surface as shown in Figure 1a. These thicknesses were estimated from tabulations of covalent and van der Waal radii<sup>31</sup> and are shown in Figure 2 as a dashed line. This hypothetical thickness plot has a slope equal to 1.3 Å per CH<sub>2</sub> group and an intercept equal to 5.6 Å. This intercept corresponds to the length of the CH<sub>3</sub>SH molecule. This model should be taken only as a limiting hypothetical case. Infrared spectroscopic evidence (see below) indicates, in fact, that the chains of the largest thiols assume an average tilt of 20–30° from the surface normal. If an average tilt of 25° is introduced into the above model, a slope of 1.1 Å per CH<sub>2</sub> group and an intercept of 5.1 Å result.

Three types of informative comparisons can be made from these data: (1) the experimental slope changes by a factor of  $\sim 3$

(28) Born, M.; Wolf, E. *Principles of Optics*; Pergamon Press: New York, 1965.

(29) Heavens, O. S. *Optical Properties of Thin Solid Films*, Dover: New York, 1965.

(30) Hansen, W. N. In *Advances in Electrochemistry and Electrochemical Engineering*, Delahey, P., Tobias, C. W., Eds.; Wiley: New York, 1973; Vol. 9.

(31) Pauling, L. *The Nature of the Chemical Bond*; Cornell University Press: Ithaca, NY, 1960.

**Table I.** Peak Positions for  $\text{CH}_3(\text{CH}_2)_n\text{SH}$  C-H Stretching Modes in Crystalline and Liquid States and Adsorbed at Gold

structural group	C-H stretching mode	peak positions <sup>a</sup> for crystalline and liquid states, $\text{cm}^{-1}$		peak positions <sup>a</sup> for $\text{CH}_3(\text{CH}_2)_n\text{SH}$ adsorbed at gold, $\text{cm}^{-1}$							
		crystalline <sup>b</sup>	liquid <sup>c</sup>	$n = 21$	$n = 17$	$n = 15$	$n = 11$	$n = 9$	$n = 7$	$n = 5$	$n = 3$
-CH <sub>2</sub> -	$\nu_a$	2918	2924	2918	2917	2918	2919	2920	2921	2921	<i>d</i>
	$\nu_s$	2851	2855	2850	2850	2850	2851	2851	2852	2852	<i>d</i>
CH <sub>3</sub> -	$\nu_a(\text{ip})$	<i>e</i>	<i>e</i>	2965	2965	2965	2965	2966	2966	2966	2966
	$\nu_a(\text{op})$	2956	2957	<i>f</i>	<i>f</i>	<i>f</i>	<i>f</i>	<i>f</i>	<i>f</i>	<i>f</i>	<i>f</i>
	$\nu_s(\text{FR})$	<i>g</i>	<i>g</i>	2937	2938	2938	2937	2938	2939	2939	2938
	$\nu_s(\text{FR})$	<i>g</i>	<i>g</i>	2879	2878	2879	2879	2878	2879	2878	2877

<sup>a</sup>Peak positions are determined as the average for four independent spectra and are accurate to within  $1 \text{ cm}^{-1}$ . Corrections for optical dispersion distortion effects of an equivalent reflection spectrum for a monolayer are less than  $1 \text{ cm}^{-1}$  for all peaks. Further details are pointed to in the text. <sup>b</sup>Crystalline-state positions determined for  $\text{CH}_3(\text{CH}_2)_{21}\text{SH}$  in KBr (see text). <sup>c</sup>Liquid-state positions determined for  $\text{CH}_3(\text{CH}_2)_7\text{SH}$  with a liquid prism cell (see text). <sup>d</sup>Peak position could not be accurately determined because of low signal-to-noise ratio. <sup>e</sup>The  $\nu_a(\text{ip})$  is masked by the strong  $\nu_a(\text{op})$  in the crystalline- and liquid-state spectra. <sup>f</sup>The position for  $\nu_a(\text{op})$  cannot be determined because of the low signal-to-noise ratio. This is a result of the orientation of this mode with respect to the surface. <sup>g</sup>Both  $\nu_s(\text{FR})$  bands are masked by the  $\nu_a(\text{CH}_2)$  band.

between  $n = 5$  and  $n = 11$ ; (2) the slope for  $n \geq 11$  is between 10 and 40% greater than that for an ideal monolayer structure, depending upon whether the ideal structure has chains perpendicular or tilted  $20\text{--}30^\circ$  to the surface, respectively; (3) the thickness values for  $n \geq 11$  are *greater* than those for an ideal limiting structure, whereas those for  $n \leq 7$  are significantly less (even for a  $20\text{--}30^\circ$  chain tilt).

The interpretation of these data in detail is complex but one or possibly a combination of two simple effects is clearly indicated: (1) the shorter chains may adopt a more tilted or less extended conformation than the longer chains, and (2) the shorter alkyl thiols may pack less densely than the longer ones. Lower packing densities would lead to lower refractive indexes and thus lower measured ellipsometric thickness than expected from the long-chain thicknesses. In either case, the ellipsometry data suggest that the structure of the short-chain  $n$ -alkyl thiol assemblies is more disordered than that of the longer chain ( $n \geq 9$ ) assemblies. Such a structure would most likely result from a combination of conformationally disordered and thermally disordered alkyl chains because of the presence of gauche kinks and weak interchain interactions, respectively.

Although the relative trends of the experimental data can be interpreted quite reasonably in terms of the above changes in monolayer structure, the direct comparison of the magnitudes of the experimental and ideal thicknesses appears complicated and indicates more subtle effects are operative. For example, a fully extended chain for  $n = 21$  should give a maximum thickness of  $31.6 \text{ \AA}$  whereas  $35.1 \text{ \AA}$  is observed. Further, for a  $20\text{--}30^\circ$  chain tilt (see next section), an upper limit of  $\sim 29 \text{ \AA}$  is calculated for an ideal film. This discrepancy is not adequately accounted for by the experimental precision. This same type of discrepancy also appears in a study of the adsorption of organo disulfides on gold<sup>32</sup> and is contrary to the good agreement between ideal and experimental film thickness reported for the adsorption of alkyl-substituted carboxylic acids on aluminum oxides.<sup>19a</sup> Two factors, which we cannot accurately evaluate, stand out as possible contributors. First, the chemisorption<sup>33</sup> may induce changes in the optical response of the gold substrate relative to the bare, unreacted substrate. Such effects could be coverage dependent. Second, as the chain length increases and the packing of the monolayer becomes more dense (see subsequent discussions), the real refractive index of the monolayer is expected to increase. For example, the value of the refractive index of the most densely packed chain should be  $\sim 1.50$ , the value for polyethylene,<sup>34</sup> as compared to the average value of 1.45 assigned to the films for the thickness calculation. If the value for the  $n = 21$  monolayer approached 1.50, the corresponding thickness value would approach  $\sim 33 \text{ \AA}$  with the experimental line in Figure 2 approaching

the hypothetical line. Single-wavelength ellipsometric measurements cannot be easily adapted to independently determine both the refractive index and film thickness for monolayer films,<sup>35</sup> and other analysis techniques are needed to address this issue in detail.

To summarize briefly, the ellipsometry data provide definite evidence of the effects of chain length on monolayer structure. The major trends of the data correlate closely with that for the IR spectroscopic and electrochemistry results in the following sections. Although the unexpectedly large thickness values for long-chain monolayers are not understood, the deviations to the thick side strongly imply the formation of high coverage, dense films for these monolayers, a conclusion consistent with the data in the following sections.

**Characterization with Infrared Spectroscopy.** In order to evaluate the contributions of chain conformation, orientation, coverage, and packing to the changes in monolayer structure as a function of chain length, IR spectroscopic measurements were made. Figure 3 shows the IR spectra in the CH stretching region for  $n = 21, 17, 9,$  and  $5$ . Spectra were obtained for all data point values of  $n$  in Figure 2, and the spectra shown in Figure 3 were selected as representative of the features of interest in this study. Similar spectra have been reported for several thiols on gold.<sup>36</sup> Band assignments, based on previous studies,<sup>19b,37-39</sup> and peak positions are given in Table I. This table also includes, for comparison, peak positions for the spectra of solid crystalline-phase  $\text{CH}_3(\text{CH}_2)_{21}\text{SH}$  and liquid-phase  $\text{CH}_3(\text{CH}_2)_7\text{SH}$ . As shown in Figure 3a, the band at  $2965 \text{ cm}^{-1}$  is assigned to the  $\text{CH}_3$  asymmetric in-plane CH stretching mode,  $\nu_a(\text{CH}_3, \text{ip})$ , and the bands at  $2937$  and  $2879 \text{ cm}^{-1}$  are assigned to the  $\text{CH}_3$  symmetric CH stretching mode,  $\nu_s(\text{CH}_3, \text{FR})$ ; this latter band is split owing to Fermi resonance interactions with the lower frequency asymmetric  $\text{CH}_3$  deformation mode.<sup>40</sup> The bands at  $2917$  and  $2850 \text{ cm}^{-1}$  are assigned to the  $\nu_a$  and  $\nu_s$   $\text{CH}_2$  modes, respectively. The  $\nu_s(\text{CH}_2)$  and  $\nu_a(\text{CH}_3)$  modes were selected for structural interpretation owing to the minimal overlap of their absorption bands with those of other modes. Plots of the peak heights of these two modes as functions of  $n$  are given in Figure 4a,b. These data are reported as the mean of four to nine samples per point, and the uncertainties are given as the standard deviation. In Figure 4a the plot of the

(35) The determination of film thicknesses from ellipsometric data is very dependent on the physical model of the sample. The usual approach is to consider the three-phase interfacial structure to consist of isotropic parallel layers. In this study there are several structural models that can be used for interpreting the data. For example, simple calculations show that an identical optical response (polarizer and analyzer null-points) would be obtained for a densely packed monolayer that is tilted  $30^\circ$  from the surface normal (Figure 1b) with an average thickness equal to  $25.2 \text{ \AA}$  as would be obtained for a  $29\text{-\AA}$  monolayer with fully extended chains that are oriented normal to the surface with approximately 80% surface coverage.

(36) Finklea, H. O.; Melendez, J. A. *Spectroscopy* **1986**, *1* (4), 47-48.

(37) Allara, D. L.; Swalen, J. J. *Phys. Chem.* **1982**, *86*, 4675-4678.

(38) Rabolt, J. F.; Burns, F. C.; Schlotter, N. E.; Swalen, J. D. *J. Chem. Phys.* **1983**, *78*, 946-952.

(39) Snyder, R. G.; Hsu, S. L.; Krimm, S. *Spectrochim. Acta, Part A* **1978**, *34*, 395-406.

(40) Hill, I. R.; Levin, I. W. *J. Chem. Phys.* **1979**, *70*, 842-851.

(32) Nuzzo, R. G.; Fusco, F.; Allara, D. L. *J. Am. Chem. Soc.* **1987**, *109*, 2358-2368.

(33) Nuzzo, R. G.; Zegarski, B. R.; Dubois, L. H. *J. Am. Chem. Soc.* **1987**, *109*, 733-740.

(34) Swalen, J. D.; Santo, R.; Take, M.; Fischer, J. *IBM J. Res. Dev.* **1977**, *21*, 169-175.

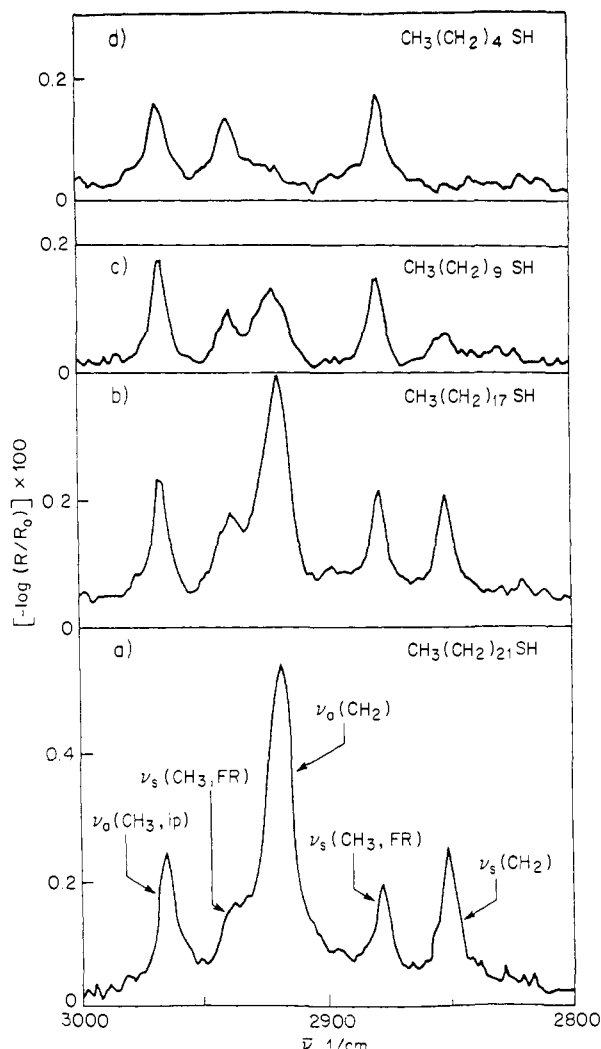


**Figure 3.** Infrared external reflection spectra for self-assembled  $n$ -alkyl thiols ( $\text{CH}_3(\text{CH}_2)_n\text{SH}$ ) at gold: (a)  $n = 21$ , (b)  $n = 17$ , (c)  $n = 9$ , and (d)  $n = 4$ . The p-polarized light was incident at  $86^\circ$ .

$\nu_a(\text{CH}_3, \text{ip})$  mode intensities from  $n = 7$  to 21 was obtained from a linear regression analysis, whereas the line connecting the data points between  $n = 3$  and  $n = 5$  is only an aid to presentation. Figure 4b shows a plot of the observed intensities of the  $\nu_s(\text{CH}_2)$  mode as a function of  $n$ . Also shown is the expected linear dependence for a structure which does not change with  $n$ , normalized to  $n = 21$ .

These data yield two immediate conclusions. First, the general agreement of the peak positions (see Table I) of the monolayer spectra with those for bulk condensed-phase alkanes<sup>39</sup> demonstrates that the structural integrity of the alkyl chains is not significantly perturbed because of the formation of the assembly. Second, the  $\text{CH}_2$  stretching mode absorption intensity is directly related to the number of  $\text{CH}_2$  units per alkyl group (Figure 4b, for example) which substantiates the major features of the ellipsometry data (see Figure 2) and indicates that the adsorption process forms reasonably uniform quality monolayers for all values of  $n$ . This conclusion eliminates solvent entrapment and multilayer formation, for example, as significant contributors to the final film structure. Under closer examination, however, these spectra indicate subtle but important effects of  $n$  on the packing density, crystalline environment, and orientation of the alkyl chains, as will be shown below.

The positions of the peak frequencies for the  $\nu_a(\text{CH}_2)$  modes in Table I provide insight into the intermolecular environment of the alkyl chains in these assemblies. Previous IR studies<sup>41,42</sup>

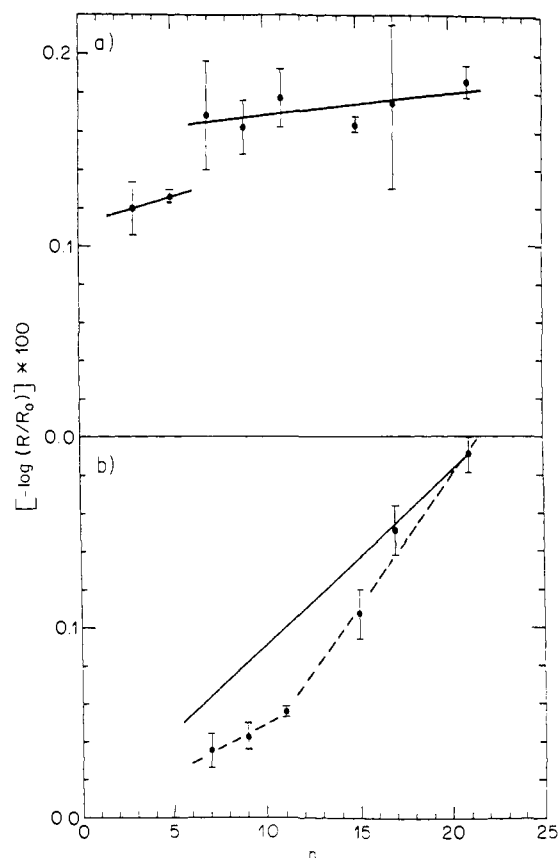


**Figure 4.** (a) Peak heights for the  $\nu_a(\text{CH}_3, \text{ip})$  vs. the number of methylene groups,  $n$ . The plot for  $n = 7$  to  $n = 21$  was determined via linear regression analysis; the plot for  $n = 3$  to  $n = 5$  serves only to aid the data discussion. (b) Peak heights for  $\nu_s(\text{CH}_2)$  vs. the number of methylene groups,  $n$ ; experimental data (---), linear interpolation from the origin to  $n = 21$  (—).

have shown that the location of these peaks are sensitive indicators for the extent of the lateral interactions between long  $n$ -alkyl and polymethylene chains. For example, the peak position for the  $\nu_a(\text{CH}_2)$  mode of a crystalline polymethylene chain ( $2920 \text{ cm}^{-1}$ ) is  $8 \text{ cm}^{-1}$  lower than that for the liquid state ( $2928 \text{ cm}^{-1}$ ), whereas for the  $\nu_s(\text{CH}_2)$  mode the peak position is  $6 \text{ cm}^{-1}$  lower in the crystalline sample ( $2850 \text{ cm}^{-1}$ ) than in the liquid ( $2856 \text{ cm}^{-1}$ ). Table I shows a similar trend for the peak frequencies for the  $\nu_a(\text{CH}_2)$  and  $\nu_s(\text{CH}_2)$  modes of bulk crystalline and liquid  $n$ -alkyl thiols. Comparison of frequencies for  $\text{CH}_3(\text{CH}_2)_{21}\text{SH}$  (in KBr) and  $\text{CH}_3(\text{CH}_2)_7\text{SH}$  (liquid) shows shifts of  $+6$  and  $+4 \text{ cm}^{-1}$  for the above modes, respectively, in changing from the solid to liquid phase.

A comparison of the peak frequencies for the  $\nu_a(\text{CH}_2)$  mode in the monolayer spectra reveals that there is a definite trend toward higher peak frequencies as the length of the alkyl chain decreases. The peak positions for the assemblies with  $n = 15$ , 17, and 21 ( $2918$ ,  $2917$ , and  $2918 \text{ cm}^{-1}$ , respectively) correspond to that of the bulk crystalline phase ( $2918 \text{ cm}^{-1}$  for  $n = 21$ ), whereas the peak position of the  $n = 5$  monolayer is  $2921 \text{ cm}^{-1}$ , a value approaching that for the pure  $n = 7$  liquid ( $2924 \text{ cm}^{-1}$ ). It is important to note that the experimental errors in assigning peak frequencies are within  $\pm 1 \text{ cm}^{-1}$  (for the average of several spectra and limited mostly due to the signal/noise levels) and that the above frequency shifts in the monolayer spectra, while small, are significant and very informative.

A similar, but less noticeable trend is observed with the  $\nu_s(\text{CH}_2)$  mode. These data indicate that in the monolayer the average local environment of an individual chain with  $15 \leq n \leq 21$  is very similar to that existing in the bulk crystalline phase, i.e., close proximity

(41) Snyder, R. G.; Strauss, H. L.; Elliger, C. A. *J. Phys. Chem.* **1982**, *86*, 5145–5150.

(42) Snyder, R. G.; Maroncelli, M.; Strauss, H. L.; Hallmark, V. M. *J. Phys. Chem.* **1986**, *90*, 5623–5630.

of neighboring chains with a tendency to minimize free volume. In contrast, for shorter chains, the average local chain environment appears similar to that of the bulk disordered or liquid phase. These data do not provide direct evidence for chain ordering in the monolayer (as a diffraction experiment might) but are quite consistent with a change in physical state of the monolayer from a higher density, crystalline-like phase with long chains to a lower density, partially disordered phase with short chains. This description is also consistent with the ellipsometry results presented earlier and will be shown to be consistent with the electrochemistry data presented later.

The crystalline-like values of the IR peak positions for the long-chain monolayers implies that the alkyl tails are fully extended with all-trans conformation. The measured intensities of the CH<sub>2</sub> stretching mode can be used to calculate an average tilt of the chain axis from the surface normal. The procedure for this type of calculation has been described in detail elsewhere<sup>19b</sup> and involves the comparison of the measured intensities with those calculated for a hypothetical isotropic monolayer. The latter were determined from the spectra of the bulk-phase thiols in a KBr matrix. The result of these calculations, which will be reported in detail elsewhere,<sup>23</sup> indicate an average tilt of 20–30° for the  $n = 15$ –21 chains. Thus, a structure similar to that in Figure 1b appears consistent with the data for the long-chain thiol monolayers. It is interesting to note that studies of di- $n$ -alkyl disulfides on polycrystalline gold indicate tilt angles of  $\sim 35^\circ$ .<sup>32</sup> Since a S atom has nearly the same diameter (within  $\sim 0.5$  Å) as the average diameter of an alkyl chain, the tilted structures require that the S-head-group spacings considerably exceed the closest approach distance (see Figure 1b). One model consistent with the larger spacings and the chain tilts would be a directed bond from a tetrahedral sulfur atom to the surface. Consideration from simple models shows that a close-packed assembly of adsorbates with such directed surface bonds could impose a tilt on the chains of  $\sim 30^\circ$  or greater and further require the S–C bond to be nearly parallel to the surface. The latter would impose an increase of the closest approach distance along the S–C axis from the S diameter of  $\sim 3.5$  Å to the largest dimension of the SCH<sub>2</sub> unit which is  $\sim 5$  Å. These arguments do not take account of any requirements of the gold surface with regard to preferred head-group spacings because of localized Au–S interactions. These interactions are not well understood,<sup>33</sup> and the further complications of the polycrystalline, multifaceted Au substrate together with surface roughness would tend to impose variability in head-group packing arrangements. These factors may force the monolayer structures to have features of both b and c in Figure 1.

The intensities of the  $\nu_a(\text{CH}_3, \text{ip})$  and  $\nu_s(\text{CH}_2)$  modes as a function of  $n$  indicate the tendency of the monolayers toward disordered structures for short chains. Figure 4a shows that for  $7 \leq n \leq 21$  the intensity of the  $\nu_a(\text{CH}_3, \text{ip})$  mode decreases negligibly with decreasing  $n$ . In contrast, the intensity decreases by  $\sim 30\%$  for  $n \leq 5$ . The  $\nu_s(\text{CH}_3)$  mode, however, as seen qualitatively from Figure 3, is fairly insensitive to  $n$ . Figure 4b shows a change in the  $\nu_s(\text{CH}_2)$  mode intensity dependence on  $n$  at  $n = 11$ . The solid line in Figure 4b connects the  $n = 21$  intensity value to the origin, representing a hypothetical set of points for a linearly decreasing film thickness with constant structure. It is important to note that the observed intensities fall *below* this normalized line.

Three chain-length-dependent factors could contribute to this observed deviation from the dependence expected for constant film structure: coverage, chain orientation, and order. The first factor is straightforward in that a loss of coverage with decreasing chain length would lead to a direct loss of total spectral intensity in excess of that expected for constant coverage. The second factor, orientation, can only account for the drop in intensities if the chains orient more perpendicular to the surface (the HCH planes of the CH<sub>2</sub> groups more parallel to the surface; see ref 19b and 43) for shorter lengths. However, this implies substantial structural order

for the short chains which is in contrast with our earlier conclusions. The last factor, a chain-length dependence of the ordering among the chains, can result in two opposing contributions to the band intensity. A decrease in the degree of ordering of alkyl chains is known to be associated with a decrease in the C–H stretching mode intensity in isotropic (e.g., randomly oriented crystallites) samples.<sup>44</sup> On the other hand, for a surface monolayer, complete disordering would randomize the orientation of the monolayer CH<sub>2</sub> groups and increase the intensity as the following argument shows. The average orientation of the  $\nu_a(\text{CH}_2)$  mode transition dipole is required to approach a value of  $54.7^\circ$  from the surface normal ( $\cos^2(54.7) = 1/3$ ) with increasing disorder. Since this transition dipole is perpendicular to the chain for a fully extended conformation, the above average CH<sub>2</sub> orientation implies an assembly of chains tilted at  $35.3^\circ$  ( $90 - 54.7^\circ$ ), a value somewhat larger than the tilt angle of 20–30° calculated from the experimental data for the long-chain monolayers. As a consequence, the introduction of a small amount of CH<sub>2</sub> group orientational disordering in the long-chain monolayers would lead to *increased* values of the CH<sub>2</sub> mode intensities (a change from 30 to  $35.4^\circ$ , the value for full disordering, gives an increase of 1.32). It is not possible from the present data to evaluate the contributions of each of these factors to the intensity deviations in Figure 4b. However, it is reasonably clear that decreasing the alkyl chain length results in the formation of a less densely packed structure. This effect should give rise in turn to chain disordering and thus more liquid-like IR spectral peak positions observed for the shorter chains.

Taken together, the ellipsometry and IR spectroscopy data are consistent with the following model. For the long-chain-length monolayers, the chains exist in a crystalline-like environment with an *average* tilt of 20–30° from the perpendicular orientation. With decreasing chain length the total attractive energy of chain–chain interactions lessens, the coverage decreases, and both the intra- and interchain order decrease. As the chain–chain interaction energy decreases with decreasing chain length, adsorbate molecules in particular low-energy surface sites are more likely to be thermally desorbed.<sup>33</sup> In general, all the data indicate that the major changes in film structure occur somewhere between  $n = 5$  and  $n = 11$ .

**Characterization with Electrochemical Methods.** The IR spectroscopy and ellipsometry results provide important information on the “average” molecular properties of the collection of adsorbed molecules, e.g., thickness, coverage, and crystalline environment. In order to probe further the average behavior of these assemblies and also to begin to examine the nature and extent of structural defects, we have exploited electrochemical measurements of heterogeneous electron transfer and differential capacitance. The former technique turns out to be highly sensitive to film defects, while the latter gives additional insight into the average structure of these assemblies.

**Heterogeneous Electron-Transfer.** Ideally, electron transfer through a closest packed monolayer of alkyl chains occurs via a highly nonadiabatic pathway in which the kinetics exhibit an exponential dependence on the separation between the electron donor and the electron acceptor.<sup>26,45</sup> As the degree of structural integrity of the monolayer decreases, owing to appearance of pin holes, grain boundaries, trapped solvent, etc., the rate, viz. the current, of heterogeneous electron transfer will be strongly increased. In certain cases the degree of integrity of the structure can be calculated with theoretical relationships for partially blocked electrodes and microelectrodes.<sup>46</sup>

For the initial electrochemical probe,  $\text{Fe}(\text{CN})_6^{3-}$  was selected since it represents a convenient and electrochemically reversible, one-electron, outer-sphere redox couple.<sup>47,48</sup> The solid line in

(44) Cameron, D. G.; Casal, H. L.; Mantsch, H. H. *Biochemistry* **1980**, *19*, 3665–3672.

(45) Albery, W. J. *Electrode Kinetics*, Clarendon: Oxford, 1975.

(46) (a) Wightman, R. M. *Anal. Chem.* **1981**, *53*, 1127A–1134A. (b) Dayton, M. A.; Brown, J. C.; Stutts, K. J.; Wightman, R. M. *Ibid.* **1980**, *52*, 946–950. (c) Amatore, C.; Saveant, J. M.; Tessier, D. *J. Electroanal. Chem.* **1983**, *147*, 39–51.

(47) Conway, B. E.; Currie, J. C. *J. Electrochem. Soc.* **1978**, *125*, 257–264.

(43) Greenler, R. G. *J. Chem. Phys.* **1966**, *44*, 310–315.

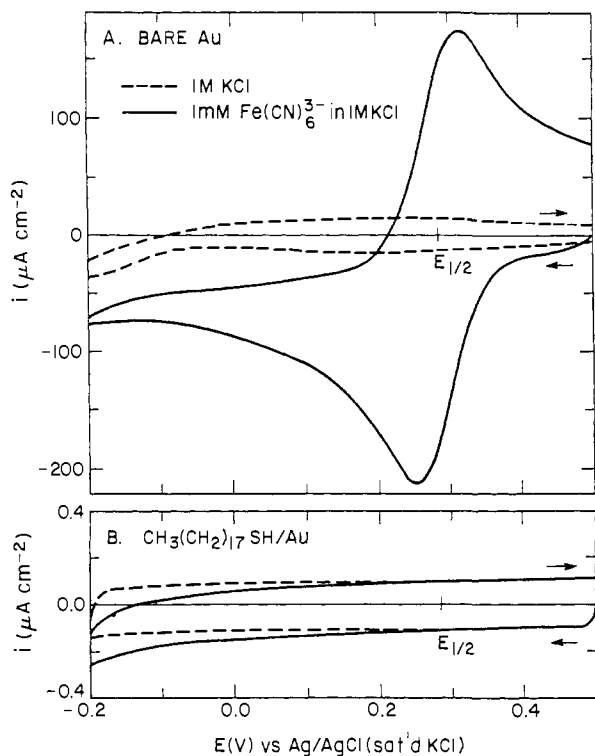


**Figure 5.** Cyclic voltammetric current response vs. applied potential for (A) bare gold and (B)  $\text{CH}_3(\text{CH}_2)_{17}\text{SH}/\text{Au}$ . The solutions are 1 mM  $\text{Fe}(\text{CN})_6^{3-}$  in 1 M KCl (—) and only 1 M KCl (---). The sweep rate is 100 mV/s.

Figure 5A shows the cyclic voltammetric current–potential ( $i$ – $E$ ) responses for bare gold with 1 mM  $\text{Fe}(\text{CN})_6^{3-}$  as the electroactive species and with 1 M KCl as the electrolyte. The dashed lines show the  $i$ – $E$  response with only 1 M KCl. Figure 5B shows the  $i$ – $E$  responses for a  $\text{CH}_3(\text{CH}_2)_{17}\text{SH}$  monolayer on gold in 1 mM  $\text{Fe}(\text{CN})_6^{3-}$  and 1 M KCl (solid line) and in only 1 M KCl (dashed line). The sweep rate is 100 mV/s. There is a dramatic difference between the  $i$ – $E$  responses for  $\text{Fe}(\text{CN})_6^{3-}$  at the monolayer-covered and bare gold electrodes. At the formal reduction potential,  $E^{\circ}$  ( $\sim 0.29$  V vs. Ag/AgCl (sat'd KCl) for  $\text{Fe}(\text{CN})_6^{3-}$ ), the Faradaic reduction current, the current due to  $\text{Fe}(\text{CN})_6^{3-}$  reduction, is less by a factor of  $>10^4$  at the modified electrode than that at bare gold. At bare gold the shapes of the  $i$ – $E$  curves and 60-mV separation between the cathodic and anodic peak currents are indicative of a diffusion-limited or electrochemically reversible one-electron redox process.<sup>49</sup> The voltammogram for the octadecyl thiol covered gold is markedly different; the current is much lower and most of the current is capacitive. The small amount of ferricyanide reduction current (compare solid and dashed lines in Figure 5b) is independent of scan direction, indicating that the reduction reaction is at steady state. In support of this conclusion, the reduction current is the same at 10 as at 100 mV/s (data not shown). This steady-state condition occurs because the small reduction currents which do flow do not allow a significant depletion of the reactant in the diffusion layer adjacent to the electrode. The data thus indicate that the reduction of  $\text{Fe}(\text{CN})_6^{3-}$  is kinetically limited.

The  $i$ – $E$  responses for the monomolecular assemblies with various alkyl chain lengths are shown in Figure 6. To examine the generality of the behavior observed with ferricyanide at the octadecyl thiol modified gold, the  $i$ – $E$  responses for  $\text{Fe}(\text{H}_2\text{O})_6^{3+}$  were obtained.  $\text{Fe}(\text{H}_2\text{O})_6^{3+}$  is an electroactive species with opposite charge and with a significantly lower heterogeneous electron-

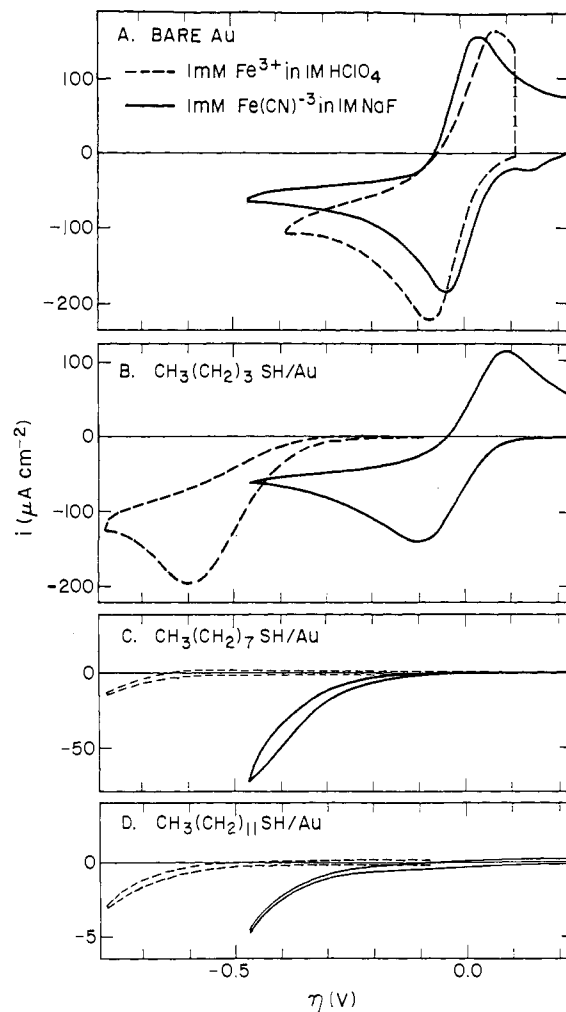


**Figure 6.** Cyclic voltammetric current response vs. over-potential for (A) bare gold, (B)  $\text{CH}_3(\text{CH}_2)_3\text{SH}/\text{Au}$ , (C)  $\text{CH}_3(\text{CH}_2)_7\text{SH}/\text{Au}$ , and (D)  $\text{CH}_3(\text{CH}_2)_{11}\text{SH}/\text{Au}$ . The solutions are 1 mM  $\text{Fe}(\text{CN})_6^{3-}$  in 1 M KCl (—) and 1 mM  $\text{Fe}(\text{H}_2\text{O})_6^{3+}$  in 1 M  $\text{HClO}_4$  (---). The sweep rate is 100 mV/s.

transfer rate constant than  $\text{Fe}(\text{CN})_6^{3-}$ . The  $i$ – $E$  responses for  $\text{Fe}(\text{CN})_6^{3-}$  (solid line) and  $\text{Fe}(\text{H}_2\text{O})_6^{3+}$  (dashed line) are shown for bare gold (Figure 6A) and for gold covered with monolayers of  $\text{CH}_3(\text{CH}_2)_3\text{SH}$  (Figure 6B),  $\text{CH}_3(\text{CH}_2)_7\text{SH}$  (Figure 6C), and  $\text{CH}_3(\text{CH}_2)_{11}\text{SH}$  (Figure 6D). The abscissa is given as the over-potential,  $\eta$ , which is the difference between the potential applied to the working electrode and the formal reduction potential. Two features are immediately apparent: (1) the cathodic currents for both couples decrease as the alkyl chain length increases, and (2) the cathodic currents for  $\text{Fe}(\text{H}_2\text{O})_6^{3+}$  are lower relative to those for  $\text{Fe}(\text{CN})_6^{3-}$  at the same modified electrode or at bare gold as expected from the lower heterogeneous rate constant for reduction of  $\text{Fe}(\text{H}_2\text{O})_6^{3+}$  compared to that for  $\text{Fe}(\text{CN})_6^{3-}$ .<sup>50</sup>

Electron transfer to solution species at these electrodes could occur in three ways: (1) the electron could transfer through the film via a tunneling process, (2) the electroactive species could permeate through the monolayer and react at the electrode surface, and (3) the electroactive species could diffuse to a bare spot, a pin hole, on the electrode. The  $i$ – $E$  responses observed for the long-chain monolayers are such that one can rule out path (2) in general and path (3) for the case of pinholes greater than the order of a micrometer.<sup>46b</sup> As described, the  $i$ – $E$  curves for both

(48) (a) Angell, D. H.; Dickinson, T. J. *Electrochem. Soc.* **1972**, *35*, 55–72. (b) Weber, J.; Samec, Z.; Marecek, V. *J. Electroanal. Chem.* **1978**, *89*, 271–288. (c) Peter, L. M.; Durr, W.; Dindra, P.; Gerischer, H. *Ibid.* **1976**, *71*, 31–50. (d) Gennett, T.; Weaver, M. J. *Anal. Chem.* **1984**, *56*, 1444–1448.

(49) Bard, A. J.; Faulkner, L. R. *Electrochemical Methods: Fundamentals and Applications*; Wiley: New York, 1980.

(50)  $\text{Ru}(\text{NH}_3)_6^{3+}$ , a well-characterized electron acceptor with a more negative  $E^{\circ}$  ( $-0.13$  V vs. Ag/AgCl (sat'd KCl)) and with very fast heterogeneous electron-transfer kinetics,<sup>58d</sup> was used for preliminary characterization of  $\text{CH}_3(\text{CH}_2)_{17}\text{SH}/\text{Au}$ . As with the other couples, extremely small reduction currents were observed, demonstrating the integrity of adsorbed thiol films on Au down to potentials of  $-0.4$  V vs. Ag/AgCl (sat'd KCl).

redox couples exhibit low cathodic currents which increase as the applied potential becomes increasingly negative. However, if the latter two pathways were dominant, the  $i$ - $E$  response would show the standard diffusion-limited characteristics for film permeation<sup>51</sup> or reaction at micro or ultramicro electrodes.<sup>46</sup> The  $i$ - $E$  responses of such processes are characterized by a sharp current rise near  $E^{\circ'}$  to a potential-independent limiting current. Alternatively, permeation of the film by the electroactive species could have an electromigration component; however, in this case, it is expected that the  $i$ - $E$  responses for  $\text{Fe}(\text{H}_2\text{O})_6^{3+}$  and  $\text{Fe}(\text{CN})_6^{3-}$  would be opposite. Reduction of the cation should be more facile than reduction of the anion. Further, reduction of the anion should become less facile, not more facile, as the potential is made more negative. A mechanism consistent with our data involves diffusion to sparsely populated surface regions where electron tunneling is more probable than for the vast majority of the surface.<sup>46c</sup>

It is apparent from this discussion that the observed electron transfer for the long alkyl chain assemblies ( $n \geq 11$ ) is limited by the presence of a nonadiabatic barrier. These results are in marked contrast to studies at "barrier" films fabricated with octadecyl siloxy groups at gold<sup>52</sup> and mixtures of octadecyl siloxy and thiol groups at gold.<sup>53</sup> Both of these latter studies report results that indicate that electron transfer is dominated by permeation of the electroactive species through the film or by pin-hole diffusion.

As stated previously, an estimate of the integrity of these assemblies can be made with the theory and experimental results for electrochemical processes at microelectrodes.<sup>46</sup> In this study we have estimated the pin-hole area by an empirical analysis using the data of Wightman and co-workers on the reduction of  $\text{Fe}(\text{CN})_6^{3-}$  at carbon disk microelectrodes at a scan rate of 100 mV/s.<sup>46b</sup> Since, for a diffusion-limited process, the current observed at a disk microelectrode represents the lowest current possible for a given electrode area, this analysis yields the maximum possible pin-hole area. For a steady-state, diffusion-limited process such as obtains at microelectrodes, the current at  $E^{\circ'}$  is half the limiting current:  $i_{1/2} = 1/2 i_{\text{lim}}$ . From the data in Figure 2C of ref 46b, the following relation was obtained:

$$i_{1/2} = 1.4 \times 10^6 rc \quad (1)$$

where  $i_{1/2}$  is in nA,  $r$  is the radius of the microelectrode in cm, and  $c$  is the concentration of the  $\text{Fe}(\text{CN})_6^{3-}$  in mol/L. In Figure 5b the reduction current at  $E^{\circ'}$  at octadecyl thiol-covered gold is less than 1 nA. (The electrode area is 0.32 cm<sup>2</sup>.) Solving for  $r$  with  $i_{1/2} < 1$  nA and  $c = 1$  mM, the maximum pin-hole radius is less than 8  $\mu\text{m}$ . This radius translates to a fractional pin-hole area less than  $6 \times 10^{-6}$  for octadecyl thiol on gold.

The variations of the reduction currents of the electroactive species in solution with overpotential and with chain length (Figure 6) agree with the predictions of simple electron-transfer theory. The currents decrease rapidly with chain length as expected for a nonadiabatic electron transfer.<sup>26</sup> Furthermore, the currents for the reductions studied ( $\text{Fe}(\text{H}_2\text{O})_6^{3+} + e^- \rightarrow \text{Fe}(\text{H}_2\text{O})_6^{2+}$  and  $\text{Fe}(\text{CN})_6^{3-} + e^- \rightarrow \text{Fe}(\text{CN})_6^{4-}$ ) show the same relative order as the same reactions measured at bare metal electrodes.<sup>48</sup> This order is maintained at alkyl thiol modified electrodes for two reasons. First, the low probability of electron tunneling through the film reduces the rate by a distance-dependent but reactant-independent factor. Secondly, the difference in the activation energies of these reactions, the major feature distinguishing them at bare electrodes,<sup>54</sup> is not affected by the intervening monolayer. Therefore, the relative order of the rates is unchanged. Unfortunately, the reduction currents show sufficient variability from sample to sample that an extensive quantitative treatment is not warranted

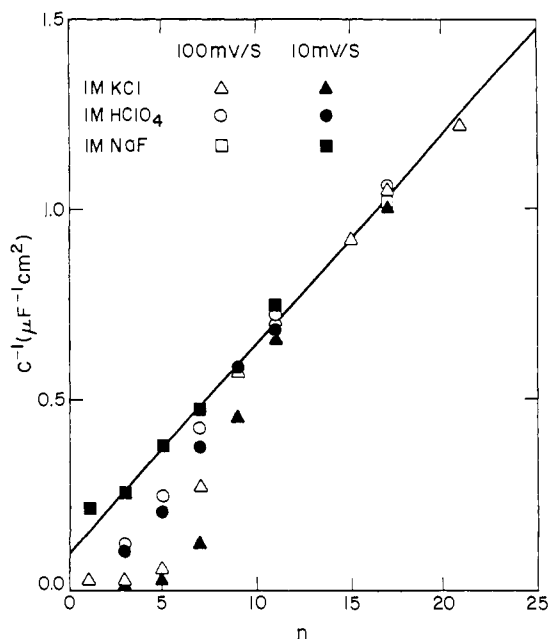


**Figure 7.** The reciprocal of capacitance at +0.3 V vs. Ag/AgCl (satd KCl) vs.  $n$  for  $\text{CH}_3(\text{CH}_2)_n\text{SH}/\text{Au}$ . The electrolytes are 1 M KCl, 1 M  $\text{HClO}_4$ , and 1 M NaF. The sweep rates are 100 and 10 mV/s.

at this time. Such variability most likely is associated with subtle variations in the monolayer coverage and degree of organizations and could be associated with experimental variables which are difficult to control such as irregularities in the underlying gold and trace contaminants in the deposition process.

**Charge Storage in the Interfacial Double Layer.** Electrochemical capacitance measurements provide another means to examine the structure of the assemblies. These, while less sensitive to the presence of defects than the electron-transfer measurements, should be consistent with the latter. More significantly, capacitance measurements provide an additional measure of film thickness as well as a probe of permeability of the films to simple ionic species. For an electrochemical double layer the differential capacitance increases with a decreasing separation between the electrode surface and the plane of closest approach for ionic charge and also increases with the polarizability of the intervening medium (with increasing dielectric constant). The capacitive current is the product of the sweep rate, differential capacitance, and electrode surface area. The  $i$ - $E$  responses in Figure 5 indicate that the capacitive current at the  $\text{CH}_3(\text{CH}_2)_{17}\text{SH}$ -covered Au electrode is a factor of 100 less than that at bare gold. This suggests that the separation of charge between the electrolyte solution and the gold substrate has increased and/or the polarizability of the separating medium has decreased. The capacitive current is essentially independent of applied potential, scan rate (10 and 100 mV/s) and electrolyte ( $\text{HClO}_4$  and NaF) (see below). This behavior, which is in marked contrast to that observed at most bare metal electrodes,<sup>55</sup> is similar to that predicted by the Helmholtz theory for the electrical double layer<sup>49</sup> which treats the interface as an ideal capacitor. Figure 7 shows the results of the generalized extension of this characterization to all of the  $n$ -alkyl thiols studied here. This plot represents the reciprocal of the differential capacitance,  $C^{-1}$ , at +0.3 V vs. Ag/AgCl (satd KCl), as a function of the length of the alkyl chain, for 1 M electrolyte solutions of KCl,  $\text{HClO}_4$ , and NaF, and at scan rates of 100 and 10 mV/s. The standard deviations for these data are comparable to or less than the size of the symbols. The solid line is a linear regression analysis of  $C^{-1}$  for  $n \geq 9$  at 100 mV/s with 1 M KCl. The slope and intercept of this line is  $0.055 \text{ cm}^2/\mu\text{F}$  per  $\text{CH}_2$  group and  $0.1 \text{ cm}^2/\mu\text{F}$ , respectively. These results clearly show that the differential capacitance for  $n \geq 9$  is inversely

(51) Ikeda, T.; Schmehl, R.; Denisevich, P.; Willman, K.; Murray, R. W. *J. Am. Chem. Soc.* **1982**, *104*, 2683-2691.

(52) Finklea, H. O.; Robinson, L. R.; Blackburn, A.; Richter, B.; Allara, D.; Bright, T. *Langmuir* **1986**, *2*, 239-244.

(53) Sagiv, J., personal communication.

(54) Hale, J. M. In *Reactions of Molecules at Surfaces*; Hush, N. S., Ed.; Wiley: New York, 1971.

(55) Delahay, P. *Double Layer and Electrode Kinetics*; Wiley: New York, 1965.

proportional to the length of the alkyl chain and independent of the electrolyte and scan rate, indicating the impervious nature (low structural defects) of these monolayers. For  $n < 9$ , these results suggest that both the  $\text{Cl}^-$  and  $\text{ClO}_4^-$  ions participate in some fashion in the charge redistribution process, demonstrating either the partial permeability of these assemblies and/or the contribution of structural defects. Qualitatively, the differences in  $C^{-1}$  for the three anions for the short-chain assemblies at gold follow the differences in the extent of specific adsorption at bare gold ( $\text{Cl}^- > \text{ClO}_4^- > \text{F}^-$ ). The apparent time dependence of the differential capacitance for the short-chain assemblies, exemplified by the differences in  $C^{-1}$  at the two scan rates, demonstrates that these structures partially act as barriers to ion transport. These differences in the rates of charge reorganization are not well understood at this time. It is also interesting to note that, in contrast to  $\text{Cl}^-$  and  $\text{ClO}_4^-$ ,  $C^{-1}$  for  $\text{F}^-$  exhibits a linear dependence on the length of the alkyl chains and is independent of scan rate. Thus, these assemblies act essentially as impermeable barriers for  $\text{F}^-$  with a low density of structural defects. The linear dependence of  $C^{-1}$  on  $n$  down to  $n = 1$  with NaF as the electrolyte suggests that the film thickness, as probed by the highly hydrated  $\text{F}^-$  anion, decreases linearly with  $n$ . This inference is consistent with the IR data in Figure 4b. As mentioned earlier, a possible explanation for the lower than expected intensity of the  $\nu_s(\text{CH}_2)$  bands for the short chains is that the coverage is decreasing but that the orientation of the chains is not changing substantially. That is, the structure has greater free volume for shorter chains. The hydrated fluoride anion could be incapable of penetrating even this open structure, whereas chloride and, to a lesser extent, perchlorate could penetrate to the gold.

As stated earlier, the capacitive behavior of these assemblies resembles that predicted by the Helmholtz theory of the electrical double layer which models the electrochemical interface as an ideal capacitor. Therefore, in view of the opportunities these assemblies may provide for fundamental studies of various electrochemical phenomena, it is worthwhile to examine the limiting features of this theory. These considerations will also serve to define the limitations of these measurements for examining the microscopic integrity of these monolayers. The Helmholtz theory models the double layer as an ideal capacitor for which the reciprocal of the capacitance (per unit area) is:

$$C^{-1} = d/\epsilon\epsilon_0 \quad (2)$$

where  $d$  is the thickness of the dielectric medium that separates the two conducting plates,  $\epsilon$  is the dielectric constant of the separation medium, and  $\epsilon_0$  is the permeativity of free space. The limitations of this theory as applied to bare metals can be understood by inspection of eq 2, which indicates that the capacitance is directly proportional to  $\epsilon$  and inversely proportional to  $d$ . However, numerous studies have shown that this theory fails to account for the variation of the capacitance as a function of the electrolyte, applied potential and the electrode composition,<sup>49</sup> suggesting that  $\epsilon$  and  $d$  are dependent on these variables. These discrepancies have, in fact, been central to the evolution of the more recent theories of the double layer at bare metals. In contrast, the behavior of these assemblies resembles that predicted by the Helmholtz theory. The  $\epsilon$  for these assemblies can be calculated, after rearranging eq 2, from the slope of the line in Figure 7. If it is assumed that the change in thickness for these assemblies as a function of chain length equals 1.3 Å per  $\text{CH}_2$  group (the value for fully extended alkyl chains packed perpendicular to the surface as in Figure 1a), then  $\epsilon$  is found to equal 2.6. This compares reasonably with the value of 2.3 for the dielectric constant of polyethylene,<sup>56</sup> confirming that these monolayer assemblies behave as a dielectric medium of approximately the expected thickness.

Several aspects of this model deserve further discussion. The model assumes ideal conductors on both sides of the dielectric. Although it is reasonable to assume the gold is nearly ideal, such an assumption cannot be made for the electrolyte. The latter is

dilute in charge carriers and thus, as predicted by the Guoy–Chapman theory,<sup>55</sup> there should be a space-charge capacitance in series with the capacitance of the dielectric film. The Guoy–Chapman theory shows that this capacitance is at a minimum at the potential of zero charge (no electrolyte space-charge) and rises at both higher and lower potentials. At the minimum, this capacitance (for 1:1 electrolyte at 25 °C in water) is:

$$C = (228 \mu\text{F cm}^{-2} \text{ M}^{-1/2})c^{1/2} \quad (3)$$

where  $c$  is the concentration of the electrolyte (see ref 49, p 407). Thus for normal ionic strengths this capacitance is quite large compared to the capacitance of the dielectric and has only a negligible effect on the total series capacitance.

An interesting corollary to the relatively large diffuse-layer (space charge) capacitance is that almost all of the potential drop from the electrode to the bulk of the solution will occur across the dielectric. The difference in potential between the outer surface of the dielectric and the bulk is 0.5% of the total potential drop for octadecyl thiol on gold with 1 M electrolyte. Thus the outer surface is essentially at the bulk potential, and the effect of this dielectric–bulk interface potential on electrode kinetics, which is frequently a serious complication at bare metals,<sup>57</sup> should be negligible for the electrodes considered here.

The model assumes a perfectly flat gold surface and accordingly our measurements of capacitance are based on the geometric surface area of the electrode. Any roughness would give larger microscopic surface areas and thus larger apparent capacitances and dielectric constants. An estimate of the actual surface area can be obtained by dividing the calculated value of the dielectric constant (Figure 6) by the value for polyethylene. The result is a roughness factor of 1.13, which is very smooth. Transmission electron micrographs (resolution of  $\sim 10$  Å) of thin sections of a  $\text{CH}_3(\text{CH}_2)_n\text{SH}/\text{Au}/\text{Cr}/\text{Si}$  sample embedded in epoxy indeed show a smooth, slowly rolling profile.<sup>58</sup>

In the above capacitance model we have used the maximal dependence of thickness on  $n$ , 1.3 Å per methylene unit. Lower values would give lower dielectric constants more in accord with the bulk value for polyethylene. The IR spectra indicate that the methylene C–H bonds are not rigorously parallel to the surface; that is, the chains are tipped away from the normal, which gives a thinner film. Using the dielectric constant of polyethylene and the slope of the line in Figure 7, a thickness of 1.12 Å per methylene or an average chain tilt of 28° is obtained, in good agreement with the IR data.

It is instructive to consider the potential effect of water partitioned into the film. Incorporated water would increase the dielectric constant and thus could be the cause of the slightly high value we observe in comparison to polyethylene. Polymeropoulos and Sagiv<sup>17</sup> have reported that water increases the capacitance of an organic aluminum (oxide) tunnel–junction structure. They observed a 10% lower capacitance in vacuo than in air. From the slope of a plot of the reciprocal capacitance vs. chain length, they obtained a dielectric constant of 2.9 for the methylene chains in vacuo.

In summary, the capacitive behavior of long-chain alkyl thiol covered gold electrodes indicates an ion-permeable, dielectric layer about as thick as the chain is long, in good agreement with the ellipsometry and IR results. With shorter chains, the impermeability and apparent dependence of thickness on chain length are the same as for long chains with NaF as the electrolyte. KCl and  $\text{HClO}_4$  electrolytes, however, show evidence of the low packing density and disorder seen by ellipsometry and by IR spectroscopy for short chains.

## Conclusions and Prospectus

The combination of experimental probes used in this study shows that spontaneously adsorbed long-chain-length  $n$ -alkyl thiol monolayers on polycrystalline gold are well-organized structures.

(56) Lanza, V. L.; Herrman, D. B. *J. Polym. Sci.* **1958**, *28*, 622–625.

(57) Parsons, R. *Advances in Electrochemistry and Electrochemical Engineering*; Delahay, P., Ed.; Interscience: New York, 1961.

(58) Porter, M. D.; Hwang, D.; Allara, D. L., unpublished results.

These structures consist of alkyl groups which, on average, experience a crystalline-like environment, are canted from the surface normal, and packed to high densities sufficient to form high-quality barriers for both electron- and ion-transfer processes. Defects in these structures would be expected because of the complex surface morphology of the polycrystalline gold including crystallographic faceting and surface roughness as well as the complexities of the thiol head-group attachment chemistry and mismatches of ideal lattice parameters for the alkyl chains and the substrate-bound head groups. However, for the case of the long-chain thiols, the van der Waals interactions of the chains appear to sustain a structure which is a very effective dielectric barrier. Shorter chain lengths promote a loss of film organization. This results in a decreased packing density and the onset of permeability by  $\text{Cl}^-$  and  $\text{ClO}_4^-$ .

This study clearly shows that significant potential exists to adapt these *n*-alkyl thiol monolayer assemblies for use as model systems for fundamental studies of heterogeneous charge-transfer, ion transport and double-layer phenomena. There are several po-

tentially fruitful modifications, not considered in this first study, that could lead to improve the properties of this model system. These include the use of smooth, single-crystal gold substrates and the optimization of adsorption conditions as well as variations in the molecular structures of the thiols. Utilization of these approaches for various applications is presently underway.

**Acknowledgment.** The authors gratefully acknowledge many valuable discussions with G. Whitesides, B. Troughton, and their co-workers at Harvard University. We thank B. Troughton for the gift of  $\text{CH}_3(\text{CH}_2)_{21}\text{SH}$ . Also acknowledged are discussions with H. Finklea and J. Sagiv in the initial stages of this study. We are particularly grateful to R. Nuzzo for critical discussions during the course of this study. The useful comments of one reviewer are acknowledged.

**Registry No.**  $\text{CH}_3\text{CH}_2\text{SH}$ , 75-08-1;  $\text{CH}_3(\text{CH}_2)_3\text{SH}$ , 109-79-5;  $\text{CH}_3(\text{CH}_2)_5\text{SH}$ , 111-31-9;  $\text{CH}_3(\text{CH}_2)_7\text{SH}$ , 111-88-6;  $\text{CH}_3(\text{CH}_2)_9\text{SH}$ , 143-10-2;  $\text{CH}_3(\text{CH}_2)_{11}\text{SH}$ , 1322-36-7;  $\text{CH}_3(\text{CH}_2)_{15}\text{SH}$ , 2917-26-2;  $\text{CH}_3(\text{CH}_2)_{17}\text{SH}$ , 2885-00-9;  $\text{CH}_3(\text{CH}_2)_{21}\text{SH}$ , 7773-83-3; Au, 7440-57-5.

## Improved Charge Separation and Photosensitized $\text{H}_2$ Evolution from Water with $\text{TiO}_2$ Particles on Colloidal $\text{SiO}_2$ Carriers

Arthur J. Frank,\*<sup>†</sup> Itamar Willner,\*<sup>†</sup> Zafrir Goren,<sup>‡</sup> and Yinon Degani<sup>‡</sup>

Contribution from the Solar Energy Research Institute, Golden, Colorado 80401, and the Department of Organic Chemistry, The Hebrew University of Jerusalem, Jerusalem 91904, Israel. Received September 25, 1986

**Abstract:** Laser flash photolysis and steady-state photolysis studies show that electrostatic interactions have a dramatic influence on the kinetics for charge separation and hydrogen production in aqueous systems (pH 9.8) of 20-nm diameter  $\text{TiO}_2$ -modified  $\text{SiO}_2$  colloids in various combinations with an electron relay, a photosensitizer, and a Pt catalyst. Either direct excitation of the semiconductor or the photosensitizer  $\text{Ru}(\text{bpy})_3^{2+}$  ( $\text{bpy} = 2,2'$ -bipyridine), electrostatically adsorbed to the colloid, initiate electron transfer to either the zwitterionic electron relay, *N,N'*-bis(3-sulfonatopropyl)-4,4'-bipyridinium ( $\text{PVS}^0$ ), or *N,N'*-bis(3-sulfonatopropyl)-2,2'-bipyridinium ( $\text{DQS}^0$ ), or methyl viologen ( $\text{MV}^{2+}$ ). The rates and quantum yields for the formation of the radical  $\text{PVS}^{\cdot-}$  anion in both the  $\text{TiO}_2\text{-SiO}_2/\text{PVS}^0$  and the  $\text{TiO}_2\text{-SiO}_2/\text{Ru}(\text{bpy})_3^{2+}/\text{PVS}^0$  systems decline with increasing ionic strength. The rate and quantum yields for  $\text{H}_2$  production in both the  $\text{TiO}_2\text{-SiO}_2/\text{DQS}^0/\text{Pt}$  and the  $\text{TiO}_2\text{-SiO}_2/\text{Ru}(\text{bpy})_3^{2+}/\text{DQS}^0/\text{Pt}$  systems also show a similar ionic strength dependence. Kinetic analysis of the data infers that repulsion of the reduced zwitterionic relay  $\text{PVS}^{\cdot-}$  and  $\text{DQS}^{\cdot-}$  from the negatively charged colloidal interface inhibits back electron transfer to both the semiconductor and the surface-attached oxidized photosensitizer  $\text{Ru}(\text{bpy})_3^{3+}$ . Formation of the cation  $\text{MV}^{\cdot+}$  radical and its back electron transfer to the semiconductor are rapid and imply that the  $\text{MV}^{2+}$  electron relay is in close proximity to the colloid. Both the photogenerated valence-band holes and the oxidized photosensitizer  $\text{Ru}(\text{bpy})_3^{3+}$  oxidize surface  $\text{Ti-O}^-$  groups of  $\text{TiO}_2$ . This redox process has the important effect of recycling the photosensitizer for further reaction. The addition of the superoxide dismutase enzyme to the oxidized  $\text{TiO}_2\text{-(SiO}_2)$  system regenerates, in part, the activity of the semiconductor to evolve  $\text{H}_2$  and to release molecular oxygen.

Light-induced electron-transfer reactions in colloidal and particulate semiconductor dispersions have become an active area of research in photochemistry.<sup>1</sup> Extensive studies have demonstrated the potential utility of semiconductor particles as light-harvesting units in the photochemical conversion and storage of solar energy. Semiconductor particles of minute size (diameters of 5–50 nm) can have high efficiencies for the photogeneration of electron-hole pairs because of the short transit time of charge carriers from the particle interior to the surface compared with the long relaxation time for charge recombination in the bulk of the semiconductor.<sup>2</sup> A crucial problem inherent to microheterogeneous systems is, however, the rapid surface recombination of photogenerated electrons and holes as well as the back electron transfer between the semiconductor and reactive intermediates formed at the semiconductor particle-liquid interface. A second obstacle to the exploitation of small semiconductor particles for photochemical solar energy conversion is the absence of materials

that not only form colloids but also have good photostability and high solar spectral response. One approach that addresses this

(1) See, for example: (a) Kraeutler, B.; Bard, A. J. *J. Am. Chem. Soc.* **1978**, *100*, 2239. (b) Duonghong, D.; Borgarello, E.; Grätzel, M. *J. Am. Chem. Soc.* **1981**, *103*, 4685. (c) Henglein, A. *Ber. Bunsenges. Phys. Chem.* **1982**, *86*, 301. (d) Fox, M. A.; Lindig, B.; Chen, C. C. *J. Am. Chem. Soc.* **1982**, *104*, 5828. (e) Grätzel, M., Ed. *Energy Resources Through Photochemistry and Catalysis*; Academic Press: New York, 1983. (f) Meissner, D.; Memming, R.; Kastening, B. *Chem. Phys. Lett.* **1983**, *96*, 34. (g) Brus, L. E. *J. Chem. Phys.* **1984**, *80*, 4403. (h) Nenadović, M. T.; Rajh, T.; Mičić, O.; Nozik, A. J. *J. Phys. Chem.* **1984**, *88*, 5827. (i) Yesodharan, E.; Yesodharan, S.; Grätzel, M. *Solar Energy Materials* **1984**, *10*, 287. (j) Mau, A. W.-H.; Huang, C.-B.; Kakuta, N.; Bard, A. J.; Campion, A.; Fox, M. A.; White, J. M.; Webber, S. E. *J. Am. Chem. Soc.* **1984**, *106*, 6537. (k) Fojtik, A.; Weller, M.; Koch, U.; Henglein, A. *Ber. Bunsenges. Phys. Chem.* **1984**, *88*, 969. (l) Kuczynski, J. P.; Milosajević, B. H.; Thomas, J. K. *J. Phys. Chem.* **1984**, *88*, 980. (m) Ramsden, J. J.; Webber, S. E.; Grätzel, M. *J. Phys. Chem.* **1985**, *89*, 2740. (n) Tricot, Y.-M.; Emeren, A.; Fendler, J. H. *J. Phys. Chem.* **1985**, *89*, 4721. (o) Harada, H.; Sakata, T.; Ueda, T. *J. Am. Chem. Soc.* **1985**, *107*, 1773. (p) Serpone, N.; Sharma, K. D.; Jamieson, M. A.; Grätzel, M.; Ramsden, J. *Chem. Phys. Lett.* **1985**, *115*, 473. (q) Kamat, P. V. *Langmuir* **1985**, *1*, 608. (r) Yanagida, S.; Mizumoto, Pac, C. *J. Am. Chem. Soc.* **1986**, *108*, 647. (s) Pelizzetti, E.; Serpone, N., Eds. *Homogeneous and Heterogeneous Photocatalysis*; D. Reidel Publishing Co.: Dordrecht, 1986.

\*Solar Energy Research Institute.

<sup>†</sup>The Hebrew University of Jerusalem.